



Exploring possible ferromagnetism of the LaAlO₃/SrTiO₃ interfaceP. Wittlich  and H. Boschker*Max Planck Institute for Solid State Research, 70569 Stuttgart, Germany*T. Asaba and L. Li *University of Michigan, Mi 48109, USA*

H. M. L. Noad, C. A. Watson, and K. A. Moler

*Stanford Institute for Materials and Energy Sciences, SLAC National Accelerator Laboratory,
2575 Sand Hill Road, Menlo Park, California 94025, USA*

D. Daraselia, D. Japaridze, and A. Shengelaya

Tbilisi State University, GE-0179 Tbilisi, Georgia

J. Wang and J. Xia

University of California at Irvine, California 92697-4575, USA

J. Mannhart*

Max Planck Institute for Solid State Research, 70569 Stuttgart, Germany

(Received 29 July 2019; published 22 October 2019)

We report on extensive investigations of magnetism at the *n*-type LaAlO₃/SrTiO₃ interface performed by utilizing a spectrum of local and integrative analytical techniques: Scanning superconducting quantum interference device microscopy, polar Kerr magnetometry, ferromagnetic resonance, and magnetic torque magnetometry. The samples originated from the same wafers. For nominally fully oxidized samples, we find that the mere presence of the conducting interface does not induce magnetism to values exceeding already present magnetic signals originating from the substrates, irrespective of the measurement technique. With the controlled introduction of oxygen vacancies, however, the different analytical techniques with their inherently different sensitivities and potential interactions with possible magnetic moments in the samples yield different results concerning the existence of magnetism. These unexpected differences obtained with the various measurement techniques are a possible source of the disagreement in the literature about the existence of ferromagnetism at LaAlO₃/SrTiO₃ interfaces.

DOI: [10.1103/PhysRevMaterials.3.104418](https://doi.org/10.1103/PhysRevMaterials.3.104418)**I. INTRODUCTION**

Understanding the fascinating properties of the conducting interface between the insulating and nonmagnetic oxides LaAlO₃ and SrTiO₃ [1] has been the topic of numerous investigations. The origin of two-dimensional (2D) conductivity at the *n*-type interface [1–5], its superconductivity [6], gate tunable metal-insulator [7] and insulator-superconductor phase transitions [8], and its Rashba spin-orbit coupling [9] have been studied, to name but a few examples. An especially intriguing aspect is the reported ferromagnetism of the interface [10–25], which for some samples has been found to coexist with superconductivity [18–20].

Numerous mechanisms have been proposed to account for magnetism emerging at the interface. Early density function theory (DFT) calculations of the electronic properties of the *n*-type LaAlO₃/SrTiO₃ interface indicated moments induced by

spin-selective filling of orbitals [26], geometrical confinement [27], or band narrowing caused by lattice modifications [28]. Kinetically driven mechanisms [29] and interactions between localized and mobile charge carriers [30–33] may also intrinsically generate net magnetic moments at the interface. In addition to these intrinsic mechanisms, defects have been identified that could cause the interface to be magnetic. The localization of charges at point defects [34] or, in a more complicated scenario, the combination of Al vacancies on the topside of the LaAlO₃ layer with band bending induced by LaAlO₃ polarization, has been found to cause a spin-selective depletion of bands [35]. Calculations exploring the influence of oxygen vacancies in various configurations [36–39] also reveal the possibility of a magnetic ground state. According to DFT calculations [36], an excess charge at the interfacial TiO₂ layer supplied by oxygen vacancies results in spin polarization. If the vacancies are located in an AlO₂ layer of the LaAlO₃ side of the interface, it causes a hybridized state close to the vacancy, similar to the mechanism proposed in Ref. [34]. Vacancies located on the topmost layer

*Corresponding author: office-mannhart@fkf.mpg.de

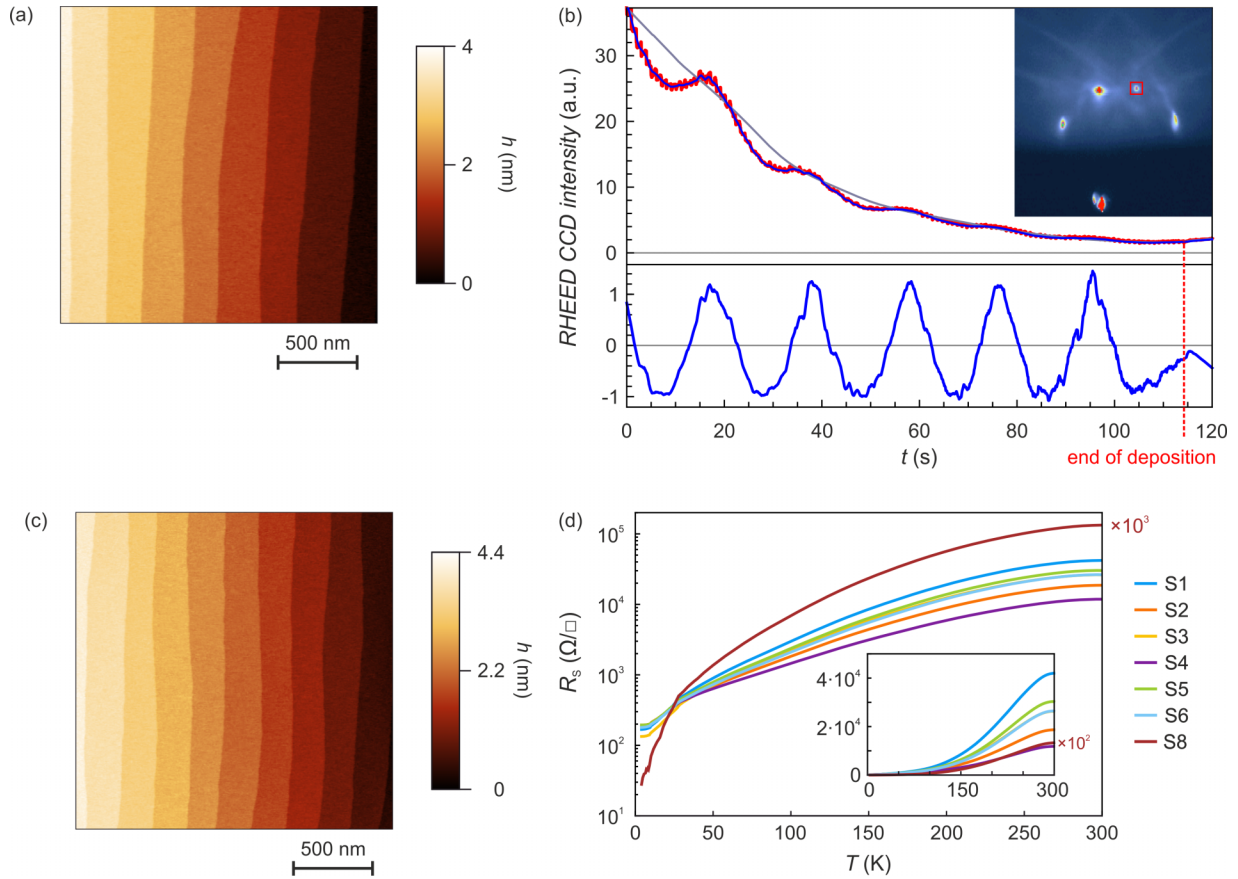


FIG. 1. Sample fabrication and characterization. (a) AFM micrograph of a SrTiO₃ substrate after the termination process. (b) RHEED oscillations of wafer 6 acquired by recording the intensity of the red area of the diffraction pattern shown in the inset. The raw signal (red) was processed as described in Ref. [53] to extract the intensity oscillations (blue). Deposition of 114 shots of LaAlO₃ was performed at $T = 640^\circ\text{C}$, $p = 8 \times 10^{-4}$ mbar, $fl. = 1.2 \text{ J/cm}^2$ and $f = 1 \text{ Hz}$. (c) AFM micrograph of wafer 1 after deposition of the LaAlO₃ layer. (d) Measured sheet resistance as a function of sample temperature (Van der Pauw). The inset depicts the data on a linear scale.

of the deposited film are energetically preferred. Likewise, the influence of an interfacial vacancy in the TiO₂ layer has been explored and found to lower the e_g orbitals below unreconstructed t_{2g} orbitals, which are then filled selectively [37]. Depending on the electron filling and defect density, a variety of magnetic or superparamagnetic regimes are found in a phase diagram of electron filling and vacancy concentration [38]. As the scope of this paper does not allow a more complete analysis of the magnetism mechanisms at n -type LaAlO₃/SrTiO₃ interfaces, we refer to the overviews in Refs. [40–46].

The possible magnetism at n -type LaAlO₃/SrTiO₃ interfaces has also been intensively explored experimentally. First experimental signatures were found in the form of hystereses in electrically measured resistance-magnetic field and resistance-temperature characteristics that were analyzed as evidence of Kondo scattering [10]. The former hystereses were later attributed to a magnetocaloric artifact [45,47]. Subsequent transport studies [11,20], scanning superconducting quantum interference device (SQUID) magnetometry [19] and torque [18] measurements demonstrated the existence of magnetism at the interface and, in several samples, the coexistence of magnetism and superconductivity. Moreover, electrical transport in combination with bulk SQUID measurements

[16,21], x-ray magnetic dichroism studies [12,13,48], laser-excited photoemission electron microscopy [17], β -nuclear magnetic resonance measurements [22], and magnetic force microscopy measurements [14,15] have all provided evidence of magnetic moments at n -type LaAlO₃/SrTiO₃ interfaces. Whereas neutron reflectometry studies [49] and other scanning SQUID measurements [50] showed the interface to be nonmagnetic. All these experiments were performed using samples that were grown and measured independently by disparate groups. No consensus regarding the magnitude, character or temperature dependence of the magnetism has yet been reached [10–25]. It is even unclear whether n -type LaAlO₃/SrTiO₃ interfaces are magnetic at all [45,49,50].

To clarify the possible existence of magnetism at an n -type (001) LaAlO₃/SrTiO₃ interface and to shed some light on the contradictory ensemble of experimental results, we have performed a systematic study in which samples cut from the same wafers were analyzed with a variety of local and nonlocal measurement techniques. For these studies, a series of samples were prepared by pulsed laser deposition under different oxidation conditions during growth, annealing and cooling procedures. Care was taken to prepare the samples in an ultraclean process that introduced as few unwanted magnetic contaminants as possible.

TABLE I. Pressures during the annealing process for all samples created for this study.

Sample	Annealing		
	p_1 (mbar) (at 600 °C)	P_2 (mbar) (at 500 °C)	P_3 (mbar) (at 400 °C)
1	10	40	400
2	8×10^{-4}	8×10^{-4}	8×10^{-4}
3	0.1	0.1	0.1
4	1×10^{-5}	1×10^{-5}	1×10^{-5}
5	4	4	4
6	4	40	400
7 ^a	4	40	400
8 ^b	8×10^{-9}	8×10^{-9}	8×10^{-9}

^aDeposition performed with excimer laser switched off.

^bDeposition performed at 8×10^{-9} mbar.

II. SAMPLE FABRICATION

As described in Ref. [51], the (001)-oriented 0.5-mm-thick SrTiO₃ substrates (SHINKOSHA CO., LTD., Japan) were terminated using HF etching followed by annealing (1000 °C, 2 h) in an oven in a stream of oxygen flowing at ambient pressure. This process results in a uniform TiO₂-covered surface, as confirmed by atomic force microscopy (AFM) [Fig. 1(a)]. Epitaxial growth was performed in a new pulsed-laser deposition chamber that was used exclusively for the LaAlO₃/SrTiO₃ growth. The wafers were placed in the system on a metallic sample holder (Haynes 25) that was in mechanical contact only with the very edge of the substrate. It was also coated with a thick layer of SrTiO₃ to reduce the risk of magnetic contamination. The substrates were heated with a CO₂ laser (9.27 μm) as described in Ref. [52]. This direct laser heating eliminates the need for thermal glue and absorber films or blocks and thus greatly reduces the risk of magnetic contamination of the samples. All but one wafer (see Table I) were grown at a pyrometrically measured substrate temperature of 640 °C and an oxygen pressure of 8×10^{-4} mbar (ramping to 640 °C in 8×10^{-4} mbar O₂). These growth parameters were fixed to preserve the growth rate and stoichiometry for all samples. After deposition of 6 u.c. of LaAlO₃ from freshly polished and preblated single crystalline targets (Crystec GmbH, Germany), which is greater than the critical thickness for creating a conducting interface [7], the wafers were cooled with three annealing steps (600, 500, and 400 °C

for 40 min each). During these steps, the wafers were annealed in an oxygen atmosphere at the pressures listed in Table I. The seemingly random variation of annealing pressure within the series was chosen to eliminate possible system drifts during the growth of the set of wafers. This sequence was also chosen to include similar wafers at the beginning and end of the series. It also includes a control wafer that underwent the identical fabrication steps as the other wafers, except that the excimer laser was not activated during the period in which the LaAlO₃ layer of the other wafers was grown. After this wafer series was grown, an additional, strongly reduced wafer was fabricated by depositing a LaAlO₃ layer at the base pressure of the system with a sample heated to the deposition temperature ($p = 8 \times 10^{-9}$ mbar, $T = 640$ °C).

The wafer surface was monitored during growth using reflection high-energy electron diffraction (RHEED). After annealing, the surface properties of the finished wafers were reexamined by AFM.

Special care was taken to avoid contamination during growth, post-growth characterization, and preparation for shipping. For example, wafers were handled exclusively with nonmetallic tweezers, placed on clean silicon wafers during measurements, and imaged with fresh AFM tips.

To cleave the wafers into samples, they were first coated with photoresist (AZ 1512 HS) to protect their surfaces. They were then placed facedown onto foil (Adwill-G17s P207) and mounted in a circular saw (DISCO DAD 321) with SiC blades (DISCO P1A851). The saw was thoroughly cleaned, then used to cut clean silicon wafers several hours before the samples were processed. To keep the wafer surface pristine, the saw cut a groove only into the back of the wafer for subsequent cleaving. The wafer surfaces were therefore never in contact with any substance used during cutting. This process enabled us to perform the first cleaning steps with the wafers still intact, then to cleave them subsequently with ease.

After the cleaving step, wafers were placed in several ultrasonic baths of distilled water, acetone, and isopropanol to remove possible contaminants. Tools and beakers were used exclusively for this wafer series. No oxygen plasma was applied to remove any remaining photoresist to avoid contamination from sputter deposition in the chamber. The samples were packed inside a glovebox for shipping. The gel boxes fixing the samples were tested to ensure they were free of magnetic contaminants.

RHEED data recorded during growth [Fig. 1(b)] were processed as described in Ref. [53]. The data confirm that

TABLE II. Electrical transport properties measured at $T = 4$ K and $\Delta B = \pm 2$ T (Van der Pauw).

Sample	R_{Sh} (Ω/□)	n_{2D} (1/cm ²)	μ (cm ² /Vs)
1	$(1.5 \pm 0.2) \times 10^2$	$(2.1 \pm 0.3) \times 10^{13}$	$(2.1 \pm 0.5) \times 10^3$
2	$(2.0 \pm 0.4) \times 10^2$	$(2.10 \pm 0.003) \times 10^{13}$	$(1.5 \pm 0.3) \times 10^3$
3	$(1.34 \pm 0.0) \times 10^2$	$(1.98 \pm 0.0) \times 10^{13}$	$(2.36 \pm 0.0) \times 10^3$
4	$(2.0 \pm 0.1) \times 10^2$	$(2.0 \pm 0.2) \times 10^{13}$	$(1.6 \pm 0.3) \times 10^3$
5	$(1.97 \pm 0.02) \times 10^2$	$(2.22 \pm 0.05) \times 10^{13}$	$(1.43 \pm 0.05) \times 10^3$
6	$(1.79 \pm 0.00) \times 10^2$	$2.4 \pm 0.0) \times 10^{13}$	$(1.46 \pm 0.00) \times 10^3$
7	–	–	–
8	$(3.3 \pm 0.20) \times 10^{-2}$	$(9.5 \pm 0.1) \times 10^{14}$	$(2.00 \pm 0.02) \times 10^4$

the stable growth conditions and the growth stop match the formation of a complete layer, considering the present phase shift of the oscillations. *Ex situ* AFM scans [Fig. 1(c)] performed on all wafers confirmed the existence of a nominally complete final layer, as there are no particles, islands or holes present on the surface of any of the wafers. Following the cleaving process described above, the edge samples of the wafers were contacted in a Van der Pauw geometry and electrically characterized in a physical property measurement system (Quantum Design). The resistance curves [Fig. 1(d)] further confirm the uniformity of the samples. Electrical transport properties of the series (Table II) show that the variation in transport is within the typical behavior of $\text{LaAlO}_3/\text{SrTiO}_3$ samples. No significant variation as a function of annealing pressure was found, except in the case of the strongly reduced wafer, which is apparently dominated by electrons supplied by oxygen vacancies. The central samples of the wafers were shipped for the magnetic measurements, with polar Kerr magnetometry having been performed on the samples previously measured by ferromagnetic resonance (FMR).

III. MEASUREMENT TECHNIQUES AND RESULTS

A. Ferromagnetic resonance

FMR measurements were performed at Tbilisi State University using a standard x-band (9.6 GHz) Bruker ER 200D-SRC EPR spectrometer. Measurements were performed within the temperature range of 90–400 K with a magnetic field orientation of between 0 and 90° to the interface normal. Magnetic field modulation and lock-in techniques were used to obtain a magnetic field derivative of the sample absorption as a function of the applied dc magnetic field. It is known that FMR is an extremely sensitive technique to detect ferromagnetic order in thin films as thin as a single atomic layer [54], allowing it to distinguish magnetic responses of a thin film and its substrate.

Independent of temperature, microwave power, and detection angle, no ferromagnetic signals were observed by FMR for any sample (for such data see the Supplemental Material [55]). Moreover, no signals indicating the presence of foreign ferromagnetic contaminants such as Fe, Ni or Co were found in any of the samples within the limit of detection of FMR 10^{10} – 10^{14} spins.

B. Scanning SQUID magnetometry

Scanning SQUID (S-SQUID) magnetometry was performed at Stanford University using S-SQUID susceptometer microscopes [56,57] in a dilution refrigerator [58] (samples 4 and 6) and in variable-temperature liquid helium cryostats (samples 2 and 8). A susceptometer with a 1.8- μm (lithographic) inner diameter pickup loop was used to measure samples 4 and 6 [56], one with a 6- μm inner diameter to measure sample 2 [57], and one with a 0.6- μm inner diameter to measure sample 8 [57].

Patches of static magnetism such as those described previously [19,23–25] were sought by collecting the dc magnetic flux signal while rastering the SQUID above the sample surface. On each sample, areas separated far from each other

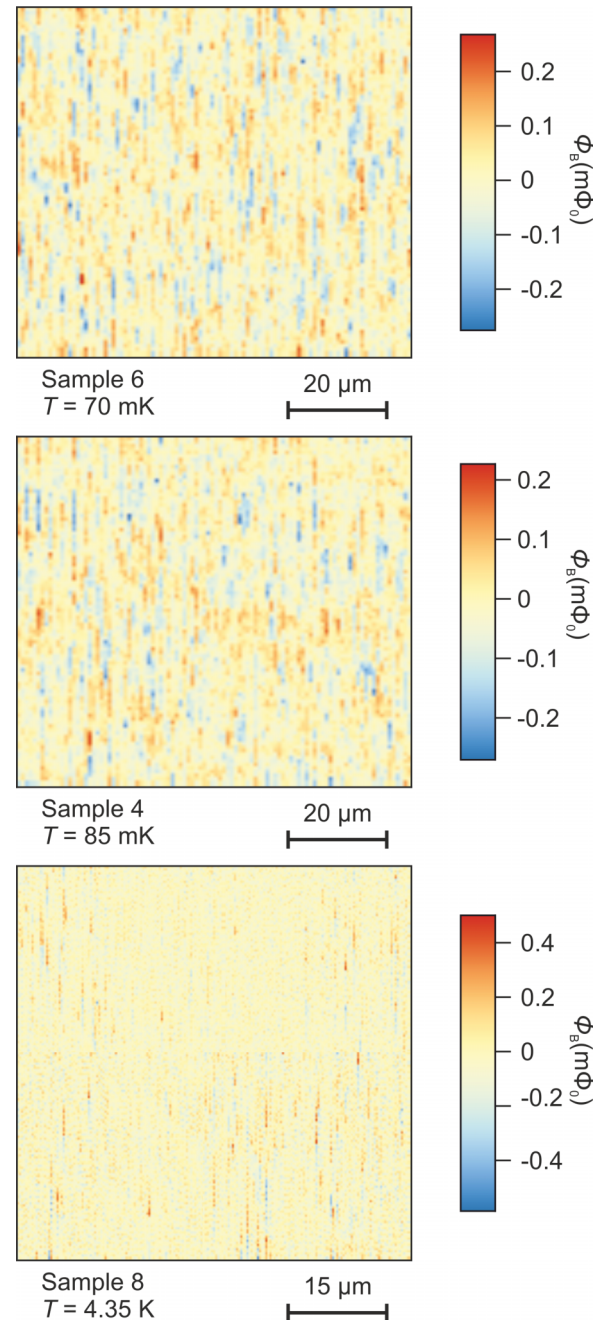


FIG. 2. S-SQUID measurements for samples of varying oxygen vacancy concentrations acquired at low temperature. Samples 4, 6, and 8 were measured with a SQUID sensor having an inner diameter pickup loop of 1.8, 1.8, and 0.6 μm , respectively. A line-by-line, second-order background fit has been subtracted from each scan. The image of Sample 8 consists of four smaller scans tiled together.

were measured to exclude local variations within the samples. The imaged area, expressed as a percentage of the total $2 \times 2 \text{ mm}^2$ sample area, was approximately 2% for sample 2, 1% for samples 4 and 6, and 0.2% for sample 8.

The S-SQUID measurements showed no traces of magnetic dipoles and no signatures of out-of-plane or in-plane magnetism above the scanning noise floor (Fig. 2), regardless

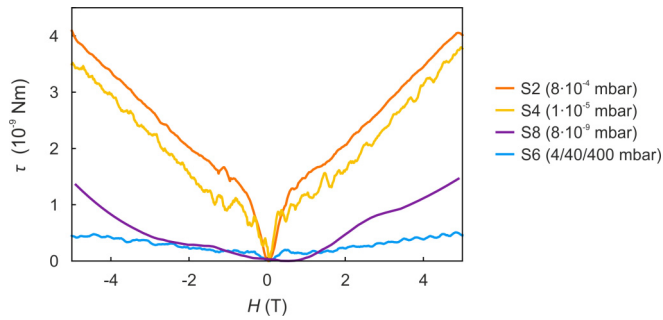


FIG. 3. Torque magnetometry signals acquired for samples 2, 4, 6, and 8 with varying oxygen vacancy concentrations. The data were acquired between 1 and 3 K.

of the measurement setup and independent of the oxygen pressure present during annealing. To set quantitative limits on possible dipole moments from the scans, the peak value of flux measured during scanning a given sample was compared to the calculated flux signal due to an isolated dipole. More details on data analysis are provided in the Supplemental Material [55]. Under conservative assumptions regarding the sensor-sample-dipole geometry, the following limits on the size of possible isolated magnetic dipoles were obtained: $8 \times 10^5 \mu_B$ for sample 2, $4.8 \times 10^6 \mu_B$ for sample 4, $3.6 \times 10^6 \mu_B$ for sample 6, and $7.9 \times 10^6 \mu_B$ for sample 8, where μ_B is the Bohr magneton. Assuming that these dipoles are located within the first unit cell of the interface these values correspond to $1.6 \times 10^{-2} - 1.58 \times 10^{-1} \mu_B/\text{unit cell}$.

Spatially inhomogeneous paramagnetism and superconductivity as described for instance in Refs. [19,25] were sought by measuring the ac magnetic susceptibility in a lock-in measurement, applying an alternating field to the sample with a field coil integrated in the sensor, and measuring the response at the lock-in frequency. Typical frequencies were of the order of kHz. After checking for and finding no gross spatial features in the susceptibility apart from patches of superconductivity, the susceptibility was measured as a function of height away from superconducting regions. The increased dwell time afforded by measuring at a single location offers increased sensitivity to potentially weak susceptibility signals, and the functional form of the height dependence can provide information on the dimensionality and moment density of the magnetism, if any exists [59].

Previous S-SQUID measurements below 1 K revealed a nonzero paramagnetic signal that decreased inversely with increasing temperature [19]. In the present work, no such signal was observed in the samples measured at similar temperatures (samples 4 and 6). From measurements of the height dependence of the susceptibility, the paramagnetic electron spin density was constrained to be no more than $1-3 \times 10^{13} \text{ cm}^{-2}$ for sample 6 and $2-6 \times 10^{13} \text{ cm}^{-2}$ for sample 4, which is one order of magnitude below the range of $1-5 \times 10^{14} \text{ cm}^{-2}$ reported in Ref. [19]. More details of the calculations are provided in the Supplemental Material [55]. Spatially inhomogeneous superconductivity was observed in both samples measured at dilution refrigerator temperatures as discussed in Ref. [60].

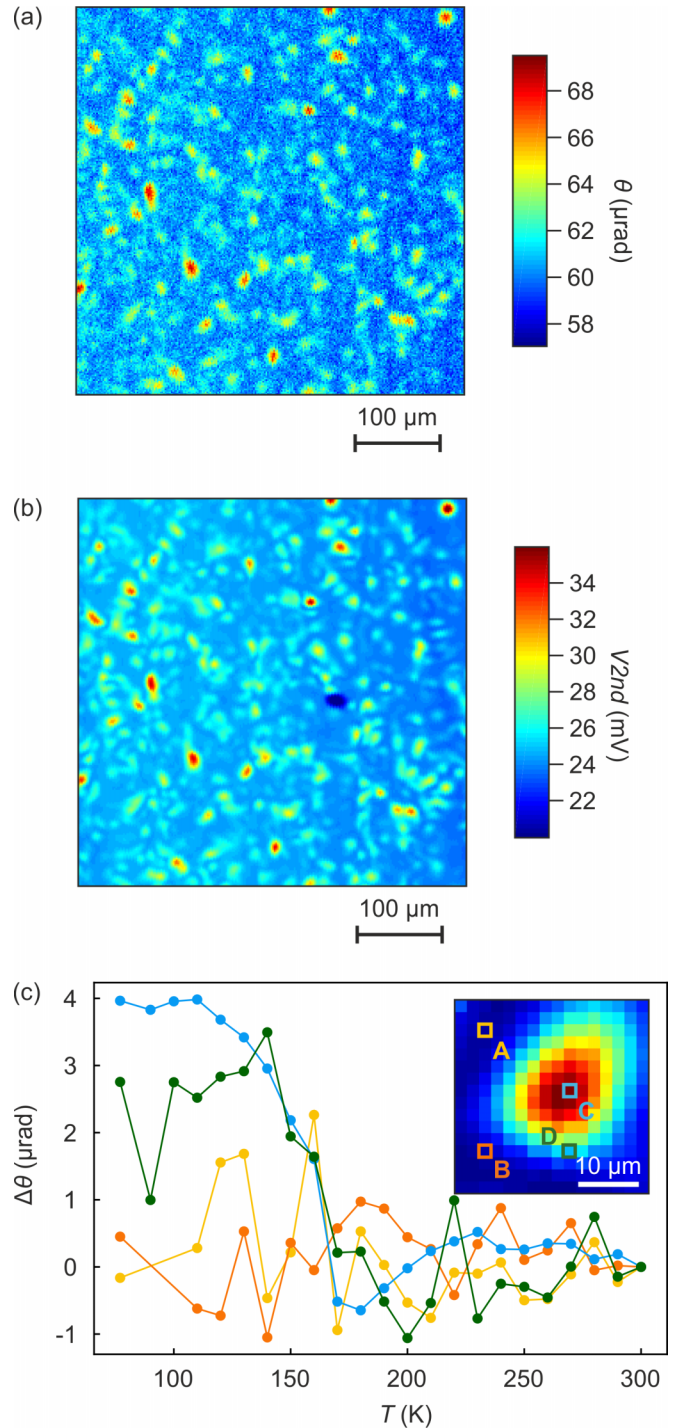


FIG. 4. Polar Kerr magnetometry. (a) Kerr rotation of Sample 6 measured at 77 K by Sagnac interferometry. (b) Reflectivity of Sample 6 measured at 77 K of the same sample area. (c) Kerr rotation measurement as a function of temperature for the pixels marked in the inset. The inset shows a close-up scan of a bright spot (reflectivity) on Sample 6.

C. Torque magnetometry

Torque magnetometry was performed at the University of Michigan using a self-built capacitive cantilever setup mounted inside a cryostat. Measurements were taken down

TABLE III. (a) Summary of techniques and measurements. (b) Summary of measurement results for all techniques used, where “n”, “n.m.” and “y” stand for “no”, “not measured” and “yes”, respectively.

	FMR	S-SQUID	Torque	Sagnac
Probing scheme	global	local	global	local
Samples measured	1–8	2,4,6,8	2,4,6,8	1,6,7,8
FM measured	FMR	S-SQUID	Torque	Sagnac
In any sample (1-8)	n	n	y	y
In fully annealed samples (1,6)	n	n	n	y
In reduced samples (2,4,8)	n	n	y	y
In bare substrate (7)	n	n.m.	n.m.	y

to 1 K with the magnetic H field oriented at adjustable angles to the interface normal. The cantilever spring constant was calibrated by the sample weight [18,61].

Torque magnetometry measurements revealed no significant signal in the fully annealed sample. In the present study, for samples annealed to create oxygen defects, pronounced torque τ signals were recorded (Fig. 3). At zero field, the $\tau - H$ curves show a sharp V-shape, indicating the magnetization quickly saturates to a finite value at low fields. This magnetization (defined as $M_T = \tau/\mu_0 H$) equals about $1.6 \mu_B$ per unit cell, normalized by the interface area. For the strongly reduced sample (Sample 6), this torque signal decreases to a much smaller value and the pronounced V-shape disappears as well (Fig. 3).

D. Polar Kerr magnetometry

Polar Kerr effect measurements were performed with a modified Sagnac interferometer [62] at the University of California at Irvine. In that instrument, magnetic fields are applied parallel to the surface normal. Light is used for probing incidents perpendicular to the surface and thus is only sensitive to the out-of-plane component of the magnetization.

In all samples, Sagnac imaging has revealed strong inhomogeneities in both optical reflectivity and magnetization (Kerr signal) [Figs. 4(a) and 4(b)]. We found that areas with higher reflectivity usually exhibit stronger magnetization, suggesting a similar yet unknown underlying mechanism. The Kerr signal was found to be strongly temperature-dependent in areas with larger reflectivity [Fig. 4(c), spots C and D], exhibiting ferromagnetic-like phase transitions. The transition

temperatures differ between samples. To explore the possibility of contamination originating from the epitaxy system or the cleaving process, two more bare substrates were tested, both of which originated from the batch used for the sample series. One of these substrates was terminated using the conventional process; the other was left untreated. Both were broken manually into suitable sizes, then thoroughly cleaned and shipped in the same manner as the other samples. Sagnac measurements on both substrates showed similar behavior: inhomogeneity in optical reflectivity and Kerr signal and ferromagnetic-like phase transitions.

An overview of the measurement techniques and samples measured with each technique is shown in Table III. A summary of the measurement results highlighting key findings is also shown in Table III.

IV. DISCUSSION

The combined data clearly reveal the difficulty of comparing results obtained with different analytical techniques. As can be seen from the conclusions listed in Table IV, the samples prepared with the ultraclean process described above are free of magnetic contamination to a level at which no significant signal can be detected for any of the analytical techniques used, except for polar Kerr magnetometry. The combined data reveal that a conducting interface in the $\text{LaAlO}_3/\text{SrTiO}_3$ heterostructure does not necessarily induce ferromagnetism. For reduced samples, however, the different techniques do produce different results, the reason for which is not completely understood. We would have expected that the samples showing a sizable torque signal would also provide a measurable magnetic signal in the scanning SQUID (see also Ref. [29] for a discussion of the origin of the torque signals). Comparing the limits established by S-SQUID to moment densities measured by bulk probes requires assumptions about the moment distribution and density in either experiment. For the sake of illustration, suppose that the $0.3\text{--}0.4 \mu_B/\text{interface}$ unit cell reported in Ref. [18] originated in dipoles spaced by approximately the diameter of the SQUID pickup loop, i.e., of the order of $1 \mu\text{m}$ (closer than was typically observed in [19,23–25].) A density of $0.3\text{--}0.4 \mu_B/\text{interface}$ unit cell with this distribution would then imply dipoles of at least $15\text{--}20 \times 10^6 \mu_B$, well above the limits set in the S-SQUID measurements described here. For reduced samples, therefore, we cannot rule out the possibility that oxygen vacancies are the source of magnetism. If oxygen vacancies were present in the oxidized samples, they did not produce a detectable

TABLE IV. Comparison of our measurement results with proposed origins of magnetism as proposed in the literature. Here “n”, “u”, “p” and “y” stand for “no”, “unlikely”, “possible” and “yes”, respectively.

	Origin of magnetism	FMR	S-SQUID	Torque	Sagnac
Intrinsic	Localized carriers [26,27]	n	n	n	u
	Itinerant carriers [28,29,32]	n	n	n	u
	Combination of both [30,31,33]	n	n	n	u
Extrinsic	Cation defects [34,35]	p	p	p	p
	Oxygen vacancies [36–39]	n	n	y	n
	Magnetic contaminations ^a	n	n	n	y

^aMagnetic contamination with respect to foreign atoms or effects originating from the substrate.

magnetic effect. High-sensitivity polar Kerr magnetometry measurements with $100 \text{ nrad/Hz}^{1/2}$ noise level [63] and 2 nrad sensitivity [64] show that patches of ferromagnetic order are present in all of the SrTiO_3 substrates obtained from Shinkosha and analyzed in the modified Sagnac interferometer setup. The data show no correlation between the magnetism of these patches and the growth or annealing procedures.

V. CONCLUSIONS

Previous research documented in the literature includes numerous experimental studies that clearly show the presence of ferromagnetism in n -type (001)-oriented $\text{LaAlO}_3/\text{SrTiO}_3$ samples. Those studies demonstrated the emergence of magnetic signatures in conjunction with the creation of the conducting interface. Moreover, the creation of oxygen vacancies or the manipulation of the interface with pressure, electric fields, and doping seemed to influence the magnetic signals within the samples. In addition, numerous theoretical models have been developed based on *ab initio* calculations that propose various mechanisms to cause magnetic ground states in the system, induced either by intrinsic effects or specific configurations of extrinsic defects.

We have analyzed possible magnetism at the $\text{LaAlO}_3/\text{SrTiO}_3$ interface using a series of wafers with conducting interfaces fabricated with an ultraclean process. The same samples were analyzed by ferromagnetic resonance, polar Kerr Magnetometry, S-SQUID microscopy, and torque magnetometry. Comparing the results obtained from the different measurement techniques has proved to be challenging because

even identical samples measured with different techniques do not necessarily provide consistent results.

We have been able to show that, to a level corresponding to sensitivity limits of the analytical techniques used, intrinsic ferromagnetism does not exist in n -type (001)-oriented $\text{LaAlO}_3/\text{SrTiO}_3$ samples. Extrinsic sources originating from the substrate or from defects such as oxygen vacancies introduced intentionally into these heterostructures are possible sources of ferromagnetic behavior shown by respective samples.

ACKNOWLEDGMENTS

We gratefully acknowledge the help of B. Baum from the crystal preparation group at the MPI in Stuttgart for her dedication and support in sample processing. We further gratefully acknowledge A. Brenner, A. Finkler, and J. Wrachtrup at the University of Stuttgart for NV-center magnetometry measurements of a fully annealed sample. The torque magnetometry work at Michigan was supported by the U.S. Department of Energy (DOE) under Award No. DE-SC0008110. Work at Stanford University was supported by the U.S. DOE, Office of Science, Basic Energy Sciences, Materials Sciences and Engineering Division, under Contract No. DE-AC02-76SF00515. H.M.L. Noad acknowledges support from a Natural Sciences and Engineering Research Council of Canada Post-Graduate Scholarship. The work at Tbilisi State University was supported by the Shota Rustaveli National Science Foundation of Georgia under Grant No. FR 17_325. The work at UC Irvine was supported by National Science Foundation Grant No. DMR-1807817.

-
- [1] A. Ohtomo and H. Y. Hwang, *Nature (London)* **427**, 423 (2004).
 - [2] W. Siemons, G. Koster, H. Yamamoto, W. A. Harrison, G. Lucovsky, T. H. Geballe, D. H. A. Blank, and M. R. Beasley, *Phys. Rev. Lett.* **98**, 196802 (2007).
 - [3] N. Nakagawa, H. Y. Hwang, and D. A. Muller, *Nat. Mater.* **5**, 204 (2006).
 - [4] M. P. Warusawithana, C. Richter, J. A. Mundy, P. Roy, J. Ludwig, S. Paetel, T. Heeg, A. A. Pawlicki, L. F. Kourkoutis, M. Zheng, M. Lee, B. Mulcahy, W. Zander, Y. Zhu, J. Schubert, J. N. Eckstein, D. A. Muller, C. S. Hellberg, J. Mannhart, and D. G. Schlom, *Nat. Commun.* **4**, 1 (2013).
 - [5] P. R. Willmott, S. A. Pauli, R. Herger, C. M. Schlepütz, D. Martoccia, B. D. Patterson, B. Delley, R. Clarke, D. Kumah, C. Cionca, and Y. Yacoby, *Phys. Rev. Lett.* **99**, 155502 (2007).
 - [6] N. Reyren, S. Thiel, A. D. Caviglia, L. F. Kourkoutis, G. Hammerl, C. Richter, C. W. Schneider, T. Kopp, A.-S. Ruetschi, D. Jaccard, M. Gabay, D. A. Muller, J.-M. Triscone, and J. Mannhart, *Science* **317**, 1196 (2007).
 - [7] S. Thiel, G. Hammerl, A. Schmehl, C. W. Schneider, and J. Mannhart, *Science* **313**, 1942 (2006).
 - [8] A. D. Caviglia, S. Gariglio, N. Reyren, D. Jaccard, T. Schneider, M. Gabay, S. Thiel, G. Hammerl, J. Mannhart, and J.-M. Triscone, *Nature (London)* **456**, 624 (2008).
 - [9] A. D. Caviglia, M. Gabay, S. Gariglio, N. Reyren, C. Cancellieri, and J. M. Triscone, *Phys. Rev. Lett.* **104**, 126803 (2010).
 - [10] A. Brinkman, M. Huijben, M. van Zalk, J. Huijben, U. Zeitler, J. C. Maan, W. G. Van der Wiel, G. Rijnders, D. H. A. Blank, and H. Hilgenkamp, *Nat. Mater.* **6**, 493 (2007).
 - [11] M. Ben Shalom, C. W. Tai, Y. Lereah, M. Sachs, E. Levy, D. Rakhmilevitch, A. Palevski, and Y. Dagan, *Phys. Rev. B* **80**, 140403 (2009).
 - [12] M. Salluzzo, S. Gariglio, D. Stornaiuolo, V. Sessi, S. Rusponi, C. Piamonteze, G. M. De Luca, M. Minola, D. Marré, A. Gadaleta, H. Brune, F. Nolting, N. B. Brookes, and G. Ghiringhelli, *Phys. Rev. Lett.* **111**, 087204 (2013).
 - [13] J.-S. Lee, Y. W. Xie, H. K. Sato, C. Bell, Y. Hikita, H. Y. Hwang, and C.-C. Kao, *Nat. Mater.* **12**, 703 (2013).
 - [14] F. Bi, M. Huang, S. Ryu, H. Lee, C. W. Bark, C. B. Eom, P. Irvin, and J. Levy, *Nat. Commun.* **5**, 1 (2014).
 - [15] F. Bi, M. Huang, H. Lee, C.-B. Eom, P. Irvin, and J. Levy, *Appl. Phys. Lett.* **107**, 082402 (2015).
 - [16] H.-L. L. Hu, L. Ao, A. Pham, D. Wang, Y. Wang, Z. Chen, C. Kong, T. T. Tan, X. Zu, and S. Li, *Adv. Mater. Interfaces* **3**, 1600547 (2016).
 - [17] Y. Motoyui, T. Taniuchi, P. Scheiderer, J. N. Lee, J. Gabel, F. Pfaff, M. Sing, M. Lippmaa, R. Claessen, and S. Shin, *J. Phys. Soc. Jpn.* **88**, 034717 (2019).
 - [18] L. Li, C. Richter, J. Mannhart, and R. C. Ashoori, *Nat. Phys.* **7**, 762 (2011).
 - [19] J. A. Bert, B. Kalisky, C. Bell, M. Kim, Y. Hikita, H. Y. Hwang, and K. A. Moler, *Nat. Phys.* **7**, 767 (2011).

- [20] D. A. Dikin, M. Mehta, C. W. Bark, C. M. Folkman, C. B. Eom, and V. Chandrasekhar, *Phys. Rev. Lett.* **107**, 056802 (2011).
- [21] Ariando, X. Wang, G. Baskaran, Z. Q. Liu, J. Huijben, J. B. Yi, A. Annadi, A. R. Barman, A. Rusydi, S. Dhar, Y. P. Feng, J. Ding, H. Hilgenkamp, and T. Venkatesan, *Nat. Commun.* **2**, 188 (2011).
- [22] Z. Salman, O. Ofer, M. Radovic, H. Hao, M. Ben Shalom, K. H. Chow, Y. Dagan, M. D. Hossain, C. D. P. Levy, W. A. MacFarlane, G. M. Morris, L. Patthey, M. R. Pearson, H. Saadaoui, T. Schmitt, D. Wang, and R. F. Kiefl, *Phys. Rev. Lett.* **109**, 257207 (2012).
- [23] B. Kalisky, J. A. Bert, B. B. Klopfer, C. Bell, H. K. Sato, M. Hosoda, Y. Hikita, H. Y. Hwang, and K. A. Moler, *Nat. Commun.* **3**, 922 (2012).
- [24] B. Kalisky, J. A. Bert, C. Bell, Y. Xie, H. K. Sato, M. Hosoda, Y. Hikita, H. Y. Hwang, and K. A. Moler, *Nano Lett.* **12**, 4055 (2012).
- [25] J. A. Bert, K. C. Nowack, B. Kalisky, H. Noad, J. R. Kirtley, C. Bell, H. K. Sato, M. Hosoda, Y. Hikita, H. Y. Hwang, and K. A. Moler, *Phys. Rev. B* **86**, 060503 (2012).
- [26] R. Pentcheva and W. E. Pickett, *Phys. Rev. B* **74**, 035112 (2006).
- [27] K. Janicka, J. P. Velev, and E. Y. Tsymlal, *J. Appl. Phys.* **103**, 07B508 (2008).
- [28] N. Ganguli and P. J. Kelly, *Phys. Rev. Lett.* **113**, 127201 (2014).
- [29] E. I. B. Rodrigues, A. A. Vargas-Paredes, M. M. Doria, and M. Cariglia, *J. Supercond. Nov. Magn.* **30**, 1327 (2017).
- [30] K. Michaeli, A. C. Potter, and P. A. Lee, *Phys. Rev. Lett.* **108**, 117003 (2012).
- [31] S. Banerjee, O. Erten, and M. Randeria, *Nat. Phys.* **9**, 626 (2013).
- [32] G. Chen and L. Balents, *Phys. Rev. Lett.* **110**, 206401 (2013).
- [33] J. Ruhman, A. Joshua, S. Ilani, and E. Altman, *Phys. Rev. B* **90**, 125123 (2014).
- [34] I. S. Elfimov, S. Yunoki, and G. A. Sawatzky, *Phys. Rev. Lett.* **89**, 216403 (2002).
- [35] L. Weston, X. Y. Cui, S. P. Ringer, and C. Stampfl, *Phys. Rev. Lett.* **113**, 186401 (2014).
- [36] N. Pavlenko, T. Kopp, E. Y. Tsymlal, G. A. Sawatzky, and J. Mannhart, *Phys. Rev. B* **85**, 020407 (2012).
- [37] N. Pavlenko, T. Kopp, E. Y. Tsymlal, J. Mannhart, and G. A. Sawatzky, *Phys. Rev. B* **86**, 064431 (2012).
- [38] N. Pavlenko, T. Kopp, and J. Mannhart, *Phys. Rev. B* **88**, 201104 (2013).
- [39] M. Behrmann and F. Lechermann, *Phys. Rev. B* **92**, 125148 (2015).
- [40] H. Chen, A. M. Kolpak, and S. Ismail-Beigi, *Adv. Mater.* **22**, 2881 (2010).
- [41] M. Gabay and J.-M. Triscone, *Nat. Phys.* **9**, 610 (2013).
- [42] J. M. D. Coey, Ariando, and W. E. Pickett, *MRS Bull.* **38**, 1040 (2013).
- [43] J. A. Sulpizio, S. Ilani, P. Irvin, and J. Levy, *Annu. Rev. Mater. Res.* **44**, 117 (2014).
- [44] Y.-Y. Pai, A. Tylan-Tyler, P. Irvin, and J. Levy, *Rep. Prog. Phys.* **81**, 036503 (2018).
- [45] J. Huijben, Ph.D. thesis, Interfacial Phenomena in Atomically Engineered LaAlO₃/SrTiO₃ Heterostructures, University of Twente (2018).
- [46] H. Noad, Ph.D. thesis, Inhomogeneity in Complex Oxides: Probing Superconductivity and Magnetism with Scanning SQUID, Stanford University (2017).
- [47] V. K. Guduru, Ph.D. thesis, Surprising Magnetotransport in Oxide Heterostructures, Radboud University Nijmegen (2014).
- [48] M. Yang, Ariando, J. Zhou, T. C. Asmara, P. Krüger, X. J. Yu, X. Wang, C. Sanchez-Hanke, Y. P. Feng, T. Venkatesan, and A. Rusydi, *ACS Appl. Mater. Interfaces* **10**, 9774 (2018).
- [49] M. R. Fitzsimmons, N. W. Hengartner, S. Singh, M. Zhernenkov, F. Y. Bruno, J. Santamaria, A. Brinkman, M. Huijben, H. J. A. Molegraaf, J. de la Venta, and I. K. Schuller, *Phys. Rev. Lett.* **107**, 217201 (2011).
- [50] T. Wijnands, Master thesis, Scanning Superconducting Quantum Interference Device Microscopy, University of Twente (2013).
- [51] G. Koster, B. L. Kropman, G. J. H. M. Rijnders, D. H. A. Blank, and H. Rogalla, *Appl. Phys. Lett.* **73**, 2920 (1998).
- [52] M. Jäger, A. Teker, J. Mannhart, and W. Braun, *Appl. Phys. Lett.* **112**, 111601 (2018).
- [53] W. Braun, *J. Cryst. Growth* **477**, 50 (2017).
- [54] J. Lindner and K. Baberschke, *J. Phys.: Condens. Matter* **15**, R193 (2003).
- [55] See Supplemental Material at <http://link.aps.org/supplemental/10.1103/PhysRevMaterials.3.104418> for further information of sample growth parameters, measurement data, and detection limits.
- [56] M. E. Huber, N. C. Koshnick, H. Bluhm, L. J. Archuleta, T. Azua, P. G. Björnsson, B. W. Gardner, S. T. Halloran, E. A. Lucero, and K. A. Moler, *Rev. Sci. Instrum.* **79**, 053704 (2008).
- [57] J. R. Kirtley, L. Paulius, A. J. Rosenberg, J. C. Palmstrom, C. M. Holland, E. M. Spanton, D. Schiessl, C. L. Jermain, J. Gibbons, Y.-K.-K. Fung, M. E. Huber, D. C. Ralph, M. B. Ketchen, G. W. Gibson, and K. A. Moler, *Rev. Sci. Instrum.* **87**, 093702 (2016).
- [58] P. G. Björnsson, B. W. Gardner, J. R. Kirtley, and K. A. Moler, *Rev. Sci. Instrum.* **72**, 4153 (2001).
- [59] J. R. Kirtley, B. Kalisky, J. A. Bert, C. Bell, M. Kim, Y. Hikita, H. Y. Hwang, J. H. Ngai, Y. Segal, F. J. Walker, C. H. Ahn, and K. A. Moler, *Phys. Rev. B* **85**, 224518 (2012).
- [60] H. Noad, P. Wittlich, J. Mannhart, and K. A. Moler, *J. Supercond. Nov. Magn.* **32**, 821 (2019).
- [61] H. Boschker, T. Harada, T. Asaba, R. Ashoori, A. V. Boris, H. Hilgenkamp, C. R. Hughes, M. E. Holtz, L. Li, D. A. Muller, H. Nair, P. Reith, X. Renshaw Wang, D. G. Schlom, A. Soukiassian, and J. Mannhart, *Phys. Rev. X* **9**, 011027 (2019).
- [62] J. Xia, P. T. Beyersdorf, M. M. Fejer, and A. Kapitulnik, *Appl. Phys. Lett.* **89**, 062508 (2006).
- [63] J. Xia, Y. Maeno, P. T. Beyersdorf, M. M. Fejer, and A. Kapitulnik, *Phys. Rev. Lett.* **97**, 167002 (2006).
- [64] X. Gong, M. Kargarian, A. Stern, D. Yue, H. Zhou, X. Jin, V. M. Galitski, V. M. Yakovenko, and J. Xia, *Sci. Adv.* **3**, e1602579 (2017).